

## Optimal semi large scale synthesis of copper and copper oxide nanoparticles by electrical explosion of wire

M. Darvishpour\*, M. Feyzi, M. Joshaghani

*Faculty of Chemistry, Razi University, P.O.Box: +98-67149, Kermanshah, Iran.*

Received June 26, 2015, Revised September 10, 2015

Copper and copper oxide nanoparticles (CNPs and CONPs) were produced in large scale by the Electrical Explosion of Wire process (EEW). Characterization of the Cu compound was carried out using TEM, EDX, XRD, FT-IR, and UV-Vis. X-ray diffraction spectroscopy was carried out to characterize the size of nanoparticles. The influences of wire diameter, feed rate, electrode distance and voltage in the exploding wire chamber on the particle size were analyzed by a design of experiments (DOE). This design was carried out using the Response Surface Methodology (RSM) that shows the particle size increases when the voltage decreases and decreases when other factors increase.

**Keywords:** Semi-large scale synthesis; copper nanoparticles; copper oxide nanoparticles; electrical explosion of wire process; response surface methodology.

### INTRODUCTION

Copper nanoparticles (CNPs) and copper oxide nanoparticles (CONPs) with uniform shape and narrow size distribution are gaining increased technical importance. Cu will gain increasing importance as is expected to be an essential component in the future nanodevices due to its excellent thermal and electrical conductivity as well as good bio-compatibility and surface enhanced Raman scattering activity, nonlinear optical devices and giant magnetic resistances at a cost much less than other nanoparticles [1-4]. The oxides of transition metals are an important class of semiconductors. Among these transition-metal oxides, copper oxide (CuO); one of the important-type semiconductors with a narrow band gap of 1.4 eV [5] has attracted much attention. CuO is used as optical switch, pigment, fungicide, metallurgy reagent, gas sensor, magnetic storage media, field emission (FE) emitter and solar cells owing to its photoconductive and photochemical properties [6,7].

The most important problem of wide application of CNPs and CONPs is the dependence of their properties on the production conditions. There are a wide variety of methods for preparation of CNPs and CONPs based on various chemical and physical techniques [4, 8, 9]. All of these methods require costly precursors, templates, and very high temperature. There is a specific need to find an economically variable method for preparing nanomaterials.

The wire explosion technique which is basically a physical vapor deposition technique has been used for the production of nanopowders due to several advantages which are: (a) ability to produce nanopowders with high purity, (b) high energy efficiency, and (c) feasibility to be used for mass production [10]. This technique can be considered to be making use of both top-down and bottom-up approaches. The generation of nanoparticles from this technique can be considered to be going through two processes as follows: (i) the top-down process during which the solid wire is disintegrated into vapor by the joule heating effect to produce a supersaturated vapor and (ii) the subsequent bottom-up process during which nanoparticles will be formed through the nucleation and subsequent growth of nuclei from the supersaturated vapor [11].

The results of experiments with underwater electrical explosion of conical arrays of copper wires are presented, too [12]. Several investigations have been carried out to determine the effect of various experimental factors on the characteristics of powder produced from the wire explosion. Some of these factors are: (i) ambient gas species and pressure [13, 14, 15] (ii) energy deposited into the wire [16-18], and (iii) initial crystalline structure of wire [19].

Many papers have been published on different aspects of this method. Although studies on these factors have been performed, literatures on optimization conditions for various effects by EEW are scanty and still not well explained. Furthermore, almost all reports focused on laboratory scale synthesis and there is no report on semi large scale synthesis of CNPs.

The objective of this study was optimization of

---

\* To whom all correspondence should be sent:  
E-mail: maryamdarvishpour@gmail.com

semi large scale selective synthesis of CNPs and CONPs based on the Electrical Explosion of Wire (EEW) by using design of experiments (DOE) with Response Surface Method (RSM) and prediction of particle size under different conditions [20].

### EXPERIMENTAL

**Material and methods:** X-ray diffraction (XRD) patterns for the samples were recorded on an Inel French, EQUINOX 3000 model X-ray diffractometer with Cu K<sub>α</sub> radiation (λ= 1.5406, 30 kV, 20 mA). Transmission electron microscopy (TEM) analyses were performed using a Jeol JEM-2100 transmission electron microscope with an accelerating voltage of 200kV. Fourier transform infrared (FT-IR) spectra were recorded as KBr pellets using a Shimadzu 470 FT-IR spectrophotometer. The optical absorption of the nanoparticles were performed using a Shimadzu double beam double mono-chromator spectrophotometer (8453) using quartz cells of 1 cm optical path in the wave-length range of 190–900 nm with a resolution of 0.5 nm. All these absorption spectra were recorded keeping air as the reference. Energy-dispersive X-ray (EDX) analyses of CNPs were carried out using a scanning electron microscope (SEM), Philips XL 30 and S-4160, with gold coating. DOE software Version 7.0.0 was used to investigate the statistical analysis of preparation of CNPs by EEW.

**Typical procedure for the synthesis of nanoparticles by EEW:** The EEW experiments were carried out using a designed apparatus for semi large scale synthesis of nanoparticles consists of a wire feeding system which continuously conducts wire into the explosion chamber with a defined rate. The main components of the apparatus have been shown in Fig. 1.

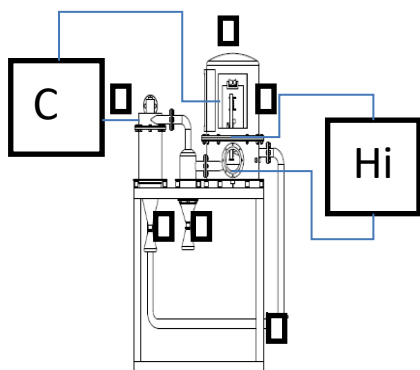


**Fig. 1.** Schematic diagram of the equipment used for manufacturing metal nanopowders via the wire electrical explosion process. 1-Evaporation chamber, 2- Wire feeding system, 3- Mesh filter of micro particles, 4- Nanoparticles collection vessel, 5- Fan, and 6- Pulse power.

After setting up, the chamber was evacuated to 0.1 Pa range and purged with argon three times. A thin wire is evaporated by passing a high current through it which is usually produced by the discharge of a capacitor bank. Due to the high-density current (10<sup>4</sup>–10<sup>6</sup> Amm<sup>-2</sup>) through the wire, the temperature of the wire rises by joule heating, followed by melting, and finally reaches the boiling point and eventually superheating of the vapor. During this heating, some surface evaporation from the wire material takes place before melting the wire completely. This surface evaporation leads to a formation of nearby plasma of the wire materials and the ambient gases, conducting a part of the total current. As the wire materials completely melt, the current through the wire decreases due to the expansion of the vapor and continues until the vapor is sufficiently thick. When the concentration of the vapor decreases to a particular value, an arc discharge occurs. At this stage, a column of ionized plasma is formed. Subsequently, the plasma begins to expand due to the enormous difference in the temperature and pressure between the plasma and the ambient gas. The expanded plasma particles are rapidly cooled down during the expansion and a supersaturated vapor is formed which undergoes a homogeneous nucleation of nanoparticles [11, 21, 22]. The nanoparticles were collected and subjected to particle size analyzing. The results were used for further statistical investigations using ANOVA analysis of variance.

### RESULTS AND DISCUSSION

**Experimental design and mathematical model:** It is difficult to obtain a model similar to the real, so it is important to analyze a large number of influences, but by careful planning of experiments to take account of economic and the duration of the experiment (23). Design of experiments is a statistical approach for modeling of an experimental response  $y$  by considering the most important effective factors  $x_1, x_2, \dots, x_k$  as shown in eq.1:

$$y = f(x_1, x_2, \dots, x_k) \quad (\text{eq. 1})$$

The experimental data obtained was used to determine the coefficients of the polynomial model with RSM (eq. 2) [24].

$$Y = \beta_0 + \beta_i X_i + \beta_j X_j + \beta_{ii} X_i^2 + \beta_{jj} X_j^2 + \beta_{ij} X_i X_j + \dots \quad (\text{eq. 2})$$

Where,  $i$  and  $j$  are the linear and quadratic indexes, respectively, and  $\beta$  is the regression coefficient.  $X_i$  and  $X_j$  are the studied independent variables.  $\beta_0$  is the interception coefficient,  $\beta_i$  and  $\beta_j$  are the linear terms and  $\beta_{ii}$  and  $\beta_{jj}$  are the quadratic

terms. P value with 95% confidence level was considered to evaluate the effectiveness of the model terms.

For Design of experiment of copper nanoparticles, four parameters containing wire diameter, feed rate, electrode distance and voltage were studied in five levels design with RSM. The ranges and levels of the variables in coded and actual units are given in Table 1. Particle size was selected as the numerical response. The experimental conditions and results obtained are shown in Table 2.

*The ANOVA results:* ANOVA results for CNPs size are presented in Table 3. The Model F-value of 10979.75 implies the model is significant. There is only a 0.01% chance that a "Model F-Value" this

large could occur due to noise. Values of Prob > F less than 0.0500 indicate all A, B, C, D terms are significant. The Lack of Fit F-value of 0.93 implies the Lack of Fit is not significant relative to the pure error. The Prediction R-Squared of 0.9992 was in reasonable agreement with the Adjusted R-Squared of 0.9993. Adequate precision was 389.217 indicating an adequate signal. Plots of the residuals in Supplementary Fig. S1 reveal that they have no obvious pattern and unusual structure. They also show equal scatter above and below the x-axis. This implies that the model proposed is adequate and there is no reason to suspect any violation [24]. Also, the validity of model was also evaluated using another graphs (Supplementary Fig. S2).

**Table 1.** Experimental range and levels of the independent variable based on ultimate design by RSM method.

Variables	unit	Range and levels				
		+2 $\alpha$	+ $\alpha$	0	- $\alpha$	-2 $\alpha$
Wire diameter (A)	mm	0.1	0.2	0.3	0.4	0.5
Feed rate (B)	cm/s	1	2	3	4	5
Electrode distance (C)	cm	1	2	3	4	5
Voltage (D)	kV	5	7.5	10	12.5	15

**Table 2.** Experimental conditions and CNPs size by EEW used in RSM design.

Run	Variables				Particle size (nm)
	A	B	C	D	
1	0.4	4	4	7.5	135.95
2	0.3	3	3	15	38.4
3	0.3	1	3	10	57.1
4	0.4	2	4	7.5	112.6
5	0.4	2	2	12.5	34.85
6	0.2	2	2	7.5	64.55
7	0.3	3	1	10	44.05
8	0.3	3	3	10	78.75
9	0.4	4	2	12.5	59.45
10	0.2	2	2	12.5	23.05
11	0.2	4	2	12.5	47.9
12	0.3	3	3	5	120.5
13	0.4	2	2	7.5	75.25
14	0.3	5	3	10	102.1
15	0.3	3	5	10	116.1
16	0.4	4	2	7.5	98.75
17	0.1	3	3	10	68.2
18	0.5	3	3	10	92
19	0.4	2	4	12.5	71.25
20	0.2	2	4	12.5	59.65
21	0.3	3	3	10	79.15
22	0.4	4	4	12.5	95.35
23	0.3	3	3	10	80.7
24	0.2	2	4	7.5	99.65
25	0.3	3	3	10	80.1
26	0.3	3	3	10	79.8
27	0.2	4	4	12.5	82.15
28	0.3	3	3	10	79.15
29	0.2	4	2	7.5	86.45
30	0.2	4	4	7.5	122.65

**Table 3.** ANOVA results for Response Surface Linear Model. <sup>a</sup>

Source	Sum of squares	df	Mean square	F value	P-value (Prob>F)
Model	21764.93	4	5441.23	1097.975	< 0.0001
A	876.04	1	876.04	176.75	< 0.0001
B	3215.54	1	3215.54	648.56	< 0.0001
C	7815.65	1	7815.65	1577.103	< 0.0001
D	9857.71	1	9857.71	1989.165	< 0.0001
Residual	12.39	5	0.50		
Lack of fit	9.76	0	0.49	0.93	0.5970
Pure error	2.63	5	0.53		
Core Total	21777.32	9			

<sup>a</sup>R-squared= 0.9994, adjusted R-squared= 0.9993, adequate precision= 389.217, Prediction R-squared= 0.9992, Coefficient of Variation (C.V.)= 0.89, Prediction error sum of squares(press)=18.04.

The modified coded equation with significant terms based on ANOVA (eq.3) indicating the contribution of main factors on the particle size.

$$\text{particulatesize} = +79.52 + 12.08A + 23.15B + 36.09C - 40.53D \quad (\text{eq. 3})$$

The results show that order of contribution of factors in the particle size follow from the following trend:

Voltage > Electrode distance > Feed rate > Wire diameter

In addition, apart from the voltage all factors show straight relationship with the particle size. The results of contour graphs indicate the particle size increases with increasing both wire diameter

and feed rate (Fig. 2a). In the other word the particle size increases with increasing electrode distance and decreasing voltage (Fig. 2b).

*Dependency of size nanoparticles on EEW conditions:* Voltage was the most effective factor on the particle size. The correlation coefficient factor for voltage was  $-0.4053$  that unlike other factor, coefficients is negative and denotes an inverse relation between the particle size and voltage. This result is in agreement with previously reports [25, 26] and is due to increase in the energy deposited (j) in the wire during the increasing the voltage (eq. 4).

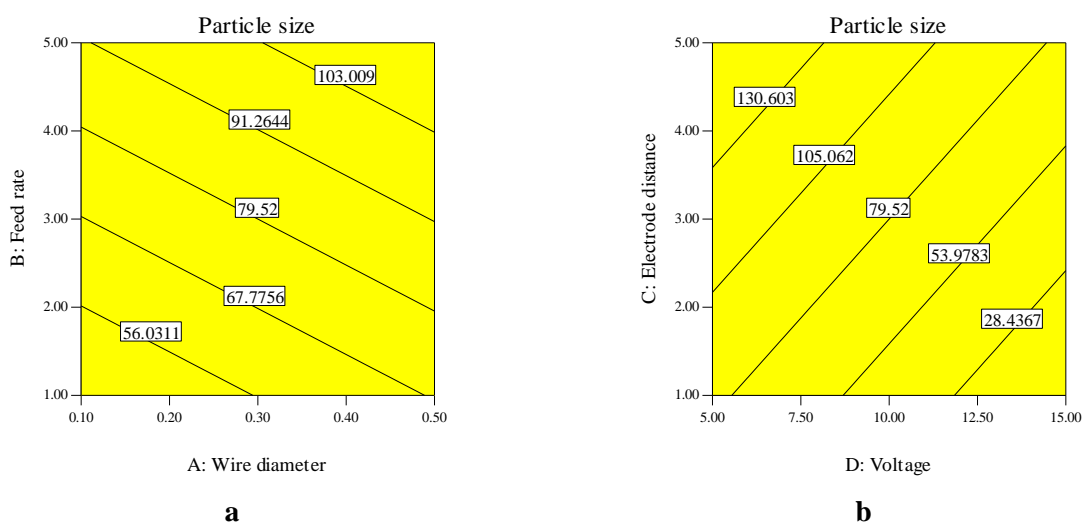


**Fig. 2.** Contour plots for nanoparticle size. Effect of wire diameter and feed rate on response. Actual factors (C=3.0, D=10) (a), electrode distance and voltage on the response. Actual factors (A=0.3, B=3) (b).

$$W_0 = \frac{1}{2} CV^2 \quad (4)$$

in where C,  $\mu\text{F}$ ; V, kV; and  $W_0$ , J are capacity, voltage and the energy stored in the capacitor, respectively. The capacitor bank of 0.1  $\mu\text{F}$  capacity was charged to a certain voltage by using an AC charger. However, the energy actually deposited to the wire, W usually is about 80–90% of the energy stored (27).

The major factor determining the particle size in the wire explosion process is superheating of the evaporated material. The particle size produced by the wire explosion process reduces substantially with increasing superheating of the metal, i.e.  $K = \frac{W}{W_s}$ , where W is the energy injected into the evaporating wire and  $W_s$  is the sublimation energy of the wire, which diminishes when the diameter of the wire is reduced.

This actual energy itself is related to the average size of particles (nm) formed as a result of EEW (Eq. 5):

$$D = 0.3 \times 10^3 (W/W_s)^{-3} \quad (5)$$

The energy for wire explosion can be written as (Eq. 6):

$$W_s = V_{\text{volume}} \cdot w_s = \frac{\pi}{4} d^2 \cdot \ell \cdot w_s \quad (6)$$

$W_s$  is the energy for sublimation of the wire per volume unit (J),  $V_{\text{volume}}$  is wire volume,  $\ell$ , length of wire (mm) and d is wire diameter (mm).  $w_s$  is specific sublimation energy of copper (47.8 J/mm<sup>3</sup>).

It was found, for example, that the energy injected to the wire, W, during the first current pulse (before the current pause) is defined by the relationship (Eq. 7):

$$W = (h_b W_0 S^2 Z)^{0.5} \quad (7)$$

that  $S = \pi d^2 / 4$  is the cross sectional area of the wire, mm<sup>2</sup>; d is the wire diameter, mm;  $Z = (L/C)^{0.5}$  is the circuit impedance, ohm; and  $h_b$  equals with eq. 8:

$$h_b = \left( \int_0^{t_3} i^2(t) dt \right) / S^2 \quad (8)$$

with the dimensionality  $\text{A}^2 \text{S} / \text{mm}^4$  and denotes the specific action before the explosion or the thermal resistance of the metal heated by a current pulse.

It can be seen from (Eq. 7) that, if  $W_0 = (h_b S^2 Z)$  and the circuit loss is neglected, then:  $W \approx W_0$ . In other words:

$$W_0 = (h_b S^2 Z) \quad (9)$$

is one of the conditions for the consistent explosion.

Considering Eq. (9), the superheating may be expressed as shown in Eq. (10):

$$K = W / w_s S l = (h_b W_0 Z)^{0.5} / w_s l \quad (10)$$

The effect of all the mentioned factors is quite clear. As K increases, the expansion rate accelerates and the degree of ionization of explosion products rises. Ions probably represent primary condensation centers. Since the vapor super-saturation is high, condensation starts at the very beginning of expansion and progresses at a maximum rate. Therefore, the increase in the expansion rate and the number of condensation centers favors the decrease in the size of particles. For a typical experiment (Run 10), we calculated particle size by using above equations that this is equal to 33 nm.

It is evident that with increasing voltage, deposited energy, and finally superheating increases and value of the particle size will be finer. In case of low  $\frac{W}{W_s}$  value the total explosion process time could be increased and thereby a growth of powder particle seemed to occur [27, 28].

With increasing electrode distance the particle size increases. Correlation coefficient factor for electrode distance is 0.3609 that denotes a linear relationship between factor and response. Its value exception voltage is larger than other factors. This means that this factor is second effective factor on particle size.

From eq.10, the effect of electrode distance is quite clear. Since overheat is inversely proportional to  $\ell$ , it is seen the K value will decrease in proportion to the increase in electrode distance that the result is that increasing the length wires.

With increasing feeding rate, particle size increases. Correlation coefficient factor for this factor is 0.2315 that is less than voltage and electrode distance effects and represents less important feed rate on particle size. A low feed rate allows a low plasma volume. This leads to low number concentration of the substance during particle growth, resulting in small nanoparticles [11].

As it is seen in Eqs. 3, 5, and 6, with increasing wire diameter,  $h_b$  decreases, consequently K decreases and the particle size increases. Correlation coefficient factor for wire diameter is 0.1208. This factor is in the fourth place, in terms of nanoparticle size. This result is compatible with the experience [28].

*Process optimization and point prediction:* There are thirty desired solutions for a selected particle size range  $25 \pm 5$  nm. The highlighted area on the overlay plot in Fig. 3 shows one of these solutions. Interestingly in this solution, the minimum required voltage was 8.84 kV while the

maximum amount of required wire diameter was 0.50 mm.

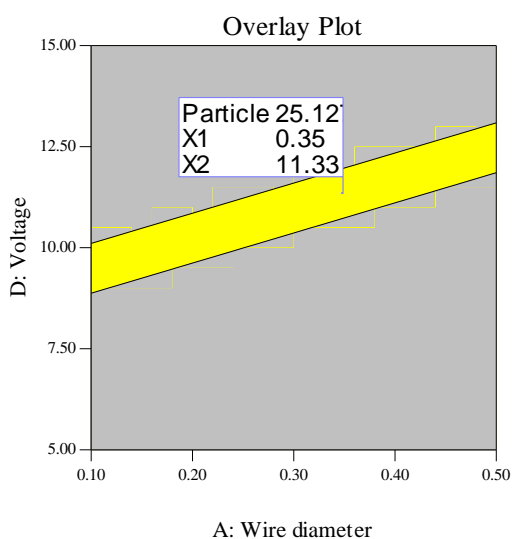


**Fig. 3.** Typically overlay plot for the optimal regions using response surface method (Actual factors: B= 1.89, C= 1.13).

An independent experiment (wire diameter, feed rate, electrode distance, and voltage = 0.2, 2, 4, and 10, respectively) was carried out to check and verify the model. The particle size measured with XRD was 80.65 nm which is in agreement with the value 79.95 nm predicted.

*Semi large scale synthesis:* In order to investigate the potent of semi large scale synthesis, the experimental run 10 was performed in the conditions (wire diameter=0.2, feed rate=2, electrode distance=2, and voltage=12.5) in 60 min. The prepared nanoparticles were collected and analyzed. The yield was 52.6 g (65%).The power

consumption was calculated about 0.5 kWh/gCu with 0.05 \$ cost (according to world electrical power average cost= 0.1 \$/1 kWh).According to this magnitude of power supply, it can be concluded that the nanoparticle prepared in this way were economically affordable compared with the other method [29].

In compare with previous studies on the EEW method for synthesis of CNPs [11, 30-32],we obtained desired particle size very selective and cost-effective.

## CHARACTERIZATION

*CNPs analyses:*Typical TEM image of CNPsis shown in Fig. 4a. The CNPswere spherical in shape. A bar graph depicting the size distribution of the CNPs was determined based on total particle population taken from TEM micrograph shown in Fig. 4b.The number-average particle size obtained 23.80 nm and the particle distribution was in the range of 10–50 nm.

A typical X-ray diffraction pattern of the prepared CNPs is shown in Supplementary Fig. S3. The major peaks located at  $2\theta$  values  $43.7^\circ$ ,  $50.7^\circ$ ,  $73.8^\circ$ ,  $90^\circ$ ,  $94.9^\circ$ are corresponded to (111), (200), (220), (311), and (222) planes of CNPs in a face-centered cubic structure (JCPDS 5-0661, $a= b =c =3.6077 \text{ \AA}$ ) respectively. In almost all experiments, no characteristic peaks related of copper oxide were observed which represents the purity of the Cu nanopowder. The average crystallite size calculated from Debye-Scherer equation was 22.3 nm [4].

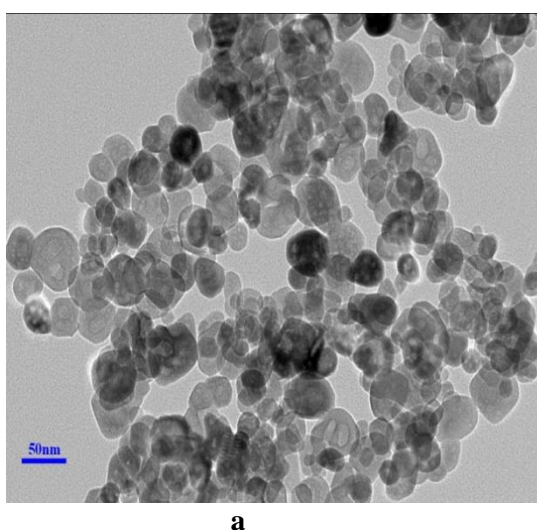


**Fig. 4.**TEM micrograph (a) and size distribution (b) of CNPs synthesized by EEW.

EDX spectroscopy (Supplementary Fig.S4) illustrated the chemical nature of synthesized CNPs

using EEW. The peak at the energy of 15keVwas attributed for copper. In addition, there are some

weak peaks belongs to O and Al. The latter impurity may be inserted due to the electrode materials.

The optical absorption spectrum of copper is shown in the Fig. 5. The SPR peak centered at 637 nm is characteristic for CNPs [33].

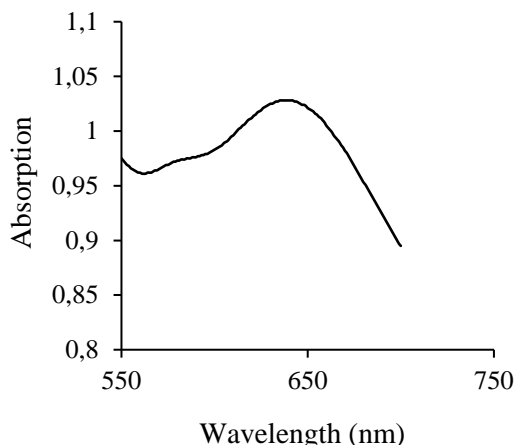


Fig. 5. UV-Visible absorption spectra of CNPs.

**CONPs Analyses:** A typical X-ray diffraction pattern of the prepared CONPs in the oxygen atmosphere is shown in Supplementary Fig. S5. The major peaks located at  $2\theta = 35.5^\circ \pm 1^\circ$ ,  $38.8^\circ \pm 1^\circ$ ,  $48.7^\circ \pm 1^\circ$ , and  $61.4^\circ \pm 1^\circ$  are corresponded to (111), (202), (020), and (220) planes of CNPs in a face-centered cubic structure CuO (JCPDS 45-0397). There are also several trace peaks in sample which were assigned to Cu<sub>2</sub>O peaks. The two highest peaks in the XRD patterns were chosen to calculate the size of the nanoparticles. This results show that the EEW is a very selective method for preparation of CONP. Calculations using Debye-Scherrer's equation showed that CuO nanoparticles had an average grain size of about 28.5 nm.

In the FT-IR spectrum of CuO (Supplementary Fig. S6), a broad band between 3800 and 3000 cm<sup>-1</sup>, centered at 3436 cm<sup>-1</sup> is assigned to OH stretching of the adsorbed water or surface OH groups. The band at 1421 cm<sup>-1</sup> is due to bending of molecular water [34]. Sharp peaks between 1000 and 500 cm<sup>-1</sup> could be assigned to Cu-O stretching.

## CONCLUSION

In conclusion, we succeeded to synthesize nanoparticles with desired size and very selective using EEW. In addition, this method is ecologically safe, provides a sufficiently high production rate, requires a relatively small energy, and allows making powders with a small degree of contamination. This method was also used in semi large scale synthesis of nanoparticles. The process has been designed and optimized using response surface methodology by which, the weight

contribution of operational conditions has been determined. The resulting coded equation was used for point prediction and verification of other experiments.

**Acknowledgments:** The authors thank the Razi University Research Council for the support of this work.

## REFERENCES

1. H. Suematsu, S. Nishimura, K. Murai, Y. Hayashi, T. Suzuki, T. Nakayama, W. Jiang, A. Yamazaki, K. Seki, *Rev. Scientific Instruments*, **78**, 6 (2007).
2. P. Kiran, G. DeNarayana, D. Rao, *Devices and Systems*, **150**, 559 (2003).
3. R. Soomro, A. Tufail, H. Sherazi, S. Juddin, S. Memon, N. Shah, M.R. Kalwar, N.H. Richard, K. Hallam, A. Sha, *Adv. Mat. Lett.*, **5**, 191 (2014).
4. T.M.D. Dang; T.T.T. Le, E. Fribourg-Blanc, M.C. Dang, *Adv. Nat. Sci. Nanosci. Nanotechnol.*, **2**, 2043 (2011).
5. S.P. Meshram, P.V. Adhyapak, U.P. Mulik, D.P. Amalnerkar, *Chem. Eng. J.*, **204**, 158 (2012).
6. A.H. MacDonald, *Nature*, **414**, 409 (2001).
7. C.L. Carnes, J.K. Stipp, K.J. Labunde, *Langmuir*, **18**, 1352 (2002).
8. Y. Lee, J. Choi, K. J. Lee, N. E. Stott, D. Kim, *Nanotechnol.*, **19**, 1361 (2008).
9. B. K. Park, S. Leong, D. Kim, J. Moon, S. Lim, J.S. Kim, *J. Colloid Interface Sci.*, **311**, 417 (2007).
10. Y. A. Kotov, *J. Nanopart. Res.*, **5**, 539 (2003).
11. Y. S. Lee, B. Bora, S. L. Yap, C. S. Wong, *Curr. Appl. Phys.*, **12**, 199 (2012).
12. D. Shafer, V.Tz. Gurovich, D. Yanuka, E. Zvulun, S. Gleizer, G. Toker, Ya.E. Krasik, *J. Appl. Phys.*, **117**, 015901 (2015).
13. R. Sarathi, T.K. Sindhu, S.R. Chakravarthy, *Mater. Charact.*, **58**, 148 (2007).
14. R. Sarathi, T. K. Sindhu, S.R. Chakravarthy, *Process. Mater. Lett.*, **61**, 1823 (2007).
15. R. Sarathi, R.S. Reddy, R.S. Tavarmani, A. Okamoto, H. Suematsu, P. Selvam, U.K. Mudali, M. Kamaraj, *IEEE Transactions on Plasma Sci.*, 93 (2015).
16. Y. Tokoi, T. Suzuki, T. Nakayama, H. Suematsu, F. Kaneko, K. Niihara, *Curr. Appl. Phys.*, **9**, S193 (2009).
17. L. Liu, J. Zhao, W. Yan, Q. Zhang, *IEEE T Nanotechnol.*, **13**, 842 (2014).
18. S. H. Tong, Z. X. Bing, Z. Shen, Z. X. Lei, W.X. Xin, *Acta Phys. Sin.*, **63**, 134 (2014).
19. V. S. Sedoi, Y. F. Ivanov, *Nanotechnology*, **19**, 1361 (2008).
20. M. Barmala, A. Mohe, R. Emadi, *J. Alloy. Comp.*, **485**, 778 (2009).
21. S. Vorob'ev, S. P. Malyshenko, S.I. Tkachenko, *High. Temp.*, **43**, 908 (2005).
22. Q. Zhou, Q. Zhang, W. Yun, X. Liu, J. Zhang, J. Zhao, L. Pang, *Transactions on Plasma Sci.*, **2**, 2198 (2012).

23. R. Abedini, S.M. Mousavi, *Chem. Ind. Chem. Eng. Q*, **18**, 171 (2012).
24. A. Asadi, A.A.L. Zinatizadeh, S. Sumathi, *Water Res.*, **46**, 4587 (2012).
25. Q. Li, Q.Z. Song, J.Z. Wang, Y.X. Duo, *Surf. Coat. Tech.*, **206**, 202 (2011).
26. L.N. Shiyan, N.A. Yavorovskii, A.V. Pustovalov, E.N. Gryaznova, *Mater. Sci. Engin.*, **81**, 012077 (2015).
27. Y.S. Kwon, Y.H. Jung, N.A. Yavorovsky, A.P. Illyn, J.S. Kim, *Scripta.mater.*, **44**, 2247 (2001).
28. P. Wankhede, P.K. Sharma, A.K. Jha, *J. Eng. Res. Appl.*, **3**, 1664 (2013).
29. I.V. Beketov, A.P. Safronov, A.V. Bagazeev, A. Larranaga, G.V. Kurlyandskaya, A.I. Medvedev, *J. Alloys Comp.*, **586**, S483 (2014).
30. P. Dash, K.Y. Balto, *J.Nanosci. Nanotechnol.*, **1**, 25 (2011).
31. R. Das, B.K. Das, *J Korean Phys. Soc.*, **61**, 710 (2012).
32. C. S. Wong, B. Bora, S.L Yap, Y.S. Lee, H. Bhuyan, M. Favre, *Curr. Appl. Phys.*, **12**, 1345 (2012).
33. M. P. Pileni, *J. Phys. Chem. B*, **108**, 20050 (2004).
34. T.M.H. Costa, M.R. Gallas, E.V. Benvenuti, J.A.H. da Jornada, *J. Phys. Chem. B*, **103**; 4278 (1999).

**Appendix.** Supplementary data

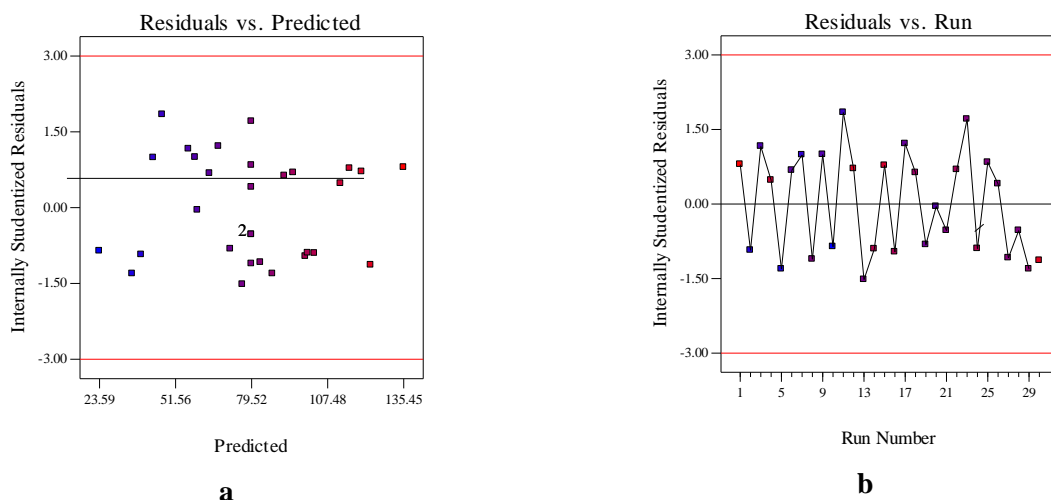


**Fig. S1.** Plot of residual vs. predicted response for ANPs size (a) and plot of residual vs. each run (b) based on preliminary design by Taguchi method.

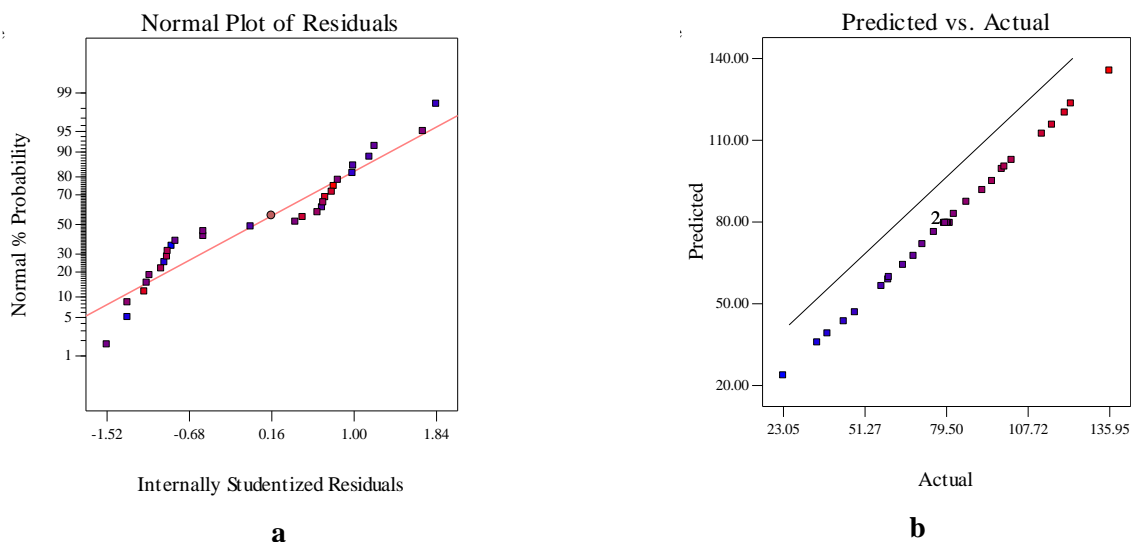


**Fig. S2.** Normal plot of residuals (a) and actual versus predicted (b) by response surface method for CNPs

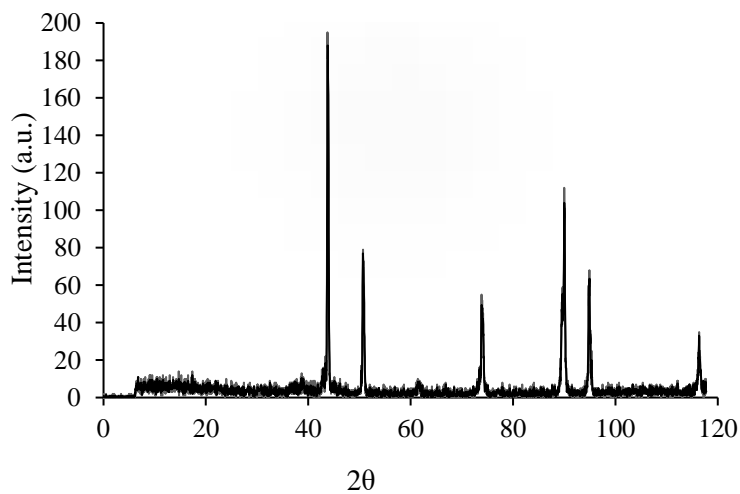


**Fig. S3.** XRD pattern of CNPs produced by EEW.

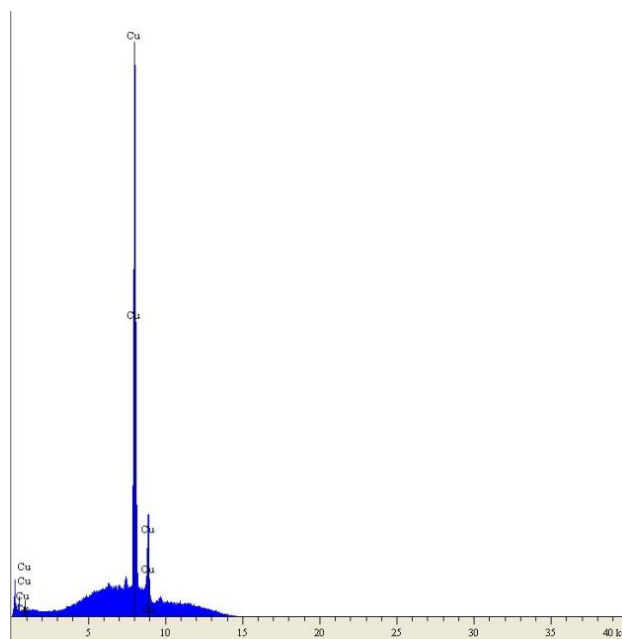


Fig. S4.EDX spectrum of CNPs synthesized by EEW.

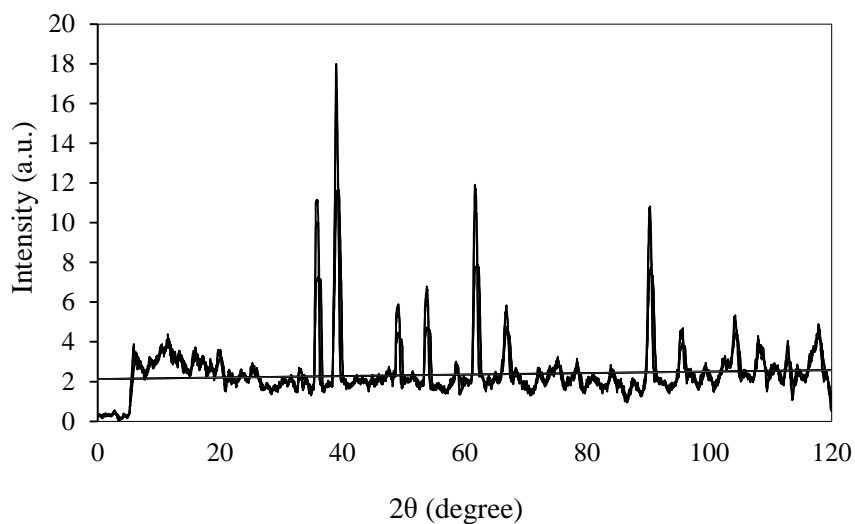


Fig. S5. XRD pattern of CONPs produced by EEW.

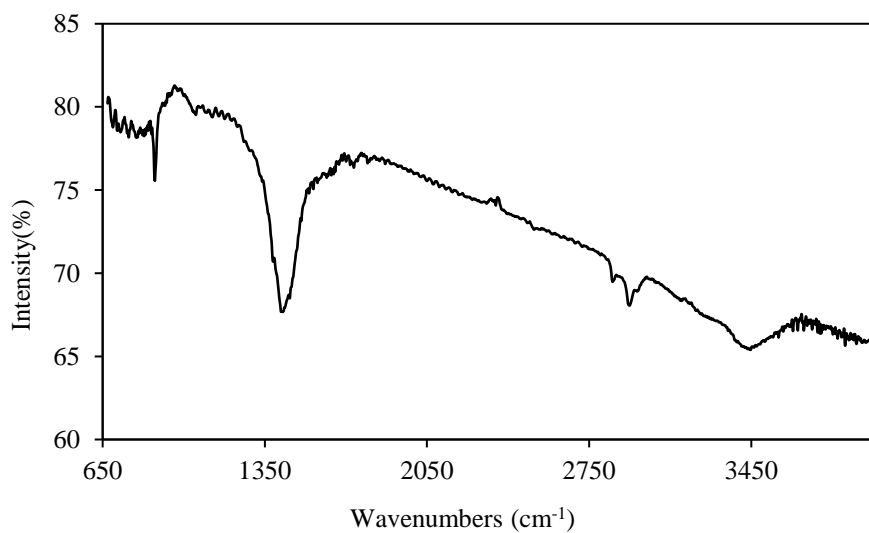


Fig. S6. FT-IR spectrum of synthesized CONPs by EEW method.